



Flow Prediction of Boundary Shear Stress and Depth Average Velocity of a Compound Channel with Narrowing Floodplain

B. Naik¹ · E. Padhi² · K. K. Khatua¹

Received: 23 February 2016 / Accepted: 9 May 2018
© Shiraz University 2018

Abstract

Prediction of boundary shear force distributions in open channel flow is crucial in many critical engineering problems such as channel design, calculation of losses and sedimentation. During floods, part of the discharge of a river is carried by the simple main channel and the rest is carried by the floodplains. For such compound channels, the flow structure becomes complicated due to the transfer of momentum between the deep main channel and the adjoining floodplains. The complexity further increases when dealing with a compound channel with non-prismatic floodplains. Knowledge of momentum transfer at the different interfaces originating from the junction between the main channel and floodplain can be acquired from the distribution of boundary shear in the subsections. The calculation of boundary shear and depth average velocity in non-prismatic compound channel flow is more complex and simple conventional approaches cannot predict the boundary shear and depth average velocity with sufficient accuracy. Hence, in this area, an easily implementable technique, the Artificial Neural Network can be used for predicting the boundary shear and depth average velocity at different sections of a converging compound channel for different geometry and flow conditions. The model's performance has lead satisfactory results. Statistical error analysis is also carried out to know the degree of accuracy of the model.

Keywords ANN · Converging angle · Depth average velocity · Non-prismatic compound channel · Relative flow depth · Velocity distribution

1 Introduction

Distribution of boundary shear stress and depth average velocity are an important aspect of river hydraulics and engineering problems such as to give a basic understanding of the resistance relationship, to understand the mechanism of sediment transport and to design stable channels, which needs to be addressed properly. Due to flow interaction between the main channel and the floodplain, the flow in a

compound section consumes more energy than a channel with simple section carrying the same flow and having the same type of channel surface. Due to continuous settlement of people near the river bank, the width of the flood plain of compound channel decreases and causes channel converging. Flood plain converging is also seen in many natural river cases. An improper estimation of floods in these regions will lead to an increase in the loss of life, and properties. The modeling of such flows is of primary importance when seeking to identify flooded areas and for flood risk management studies, etc. A strong interaction has always existed between the deep main channel and shallow floodplain, even for a prismatic compound channel. In non-prismatic compound channels with converging floodplains, due to continuous change in floodplain geometry along the flow path, the resulting interactions and momentum exchanges are further increased (Bousmar et al. 2004; Proust et al. 2006; Rezaei and Knight 2011). This extra momentum exchange is a very important parameter and should be taken into account in the overall flow

✉ B. Naik
banditanaik1982@gmail.com

E. Padhi
ellora.padhi@yahoo.co.in

K. K. Khatua
kkkhatua@yahoo.com

¹ Department of Civil Engineering, National Institute of Technology, Rourkela, India

² Department of Civil Engineering, Indian Institute of Technology, Kharagpur, India

modeling of a spatially varied river flow. The boundary shear stress distribution, velocity distribution and flow resistance in compound cross-section channels have been investigated by a number of authors (Ghosh and Jena 1971; Myers 1987; Rhodes and Knight 1994; Patra 2004; Patra and Kar 2000; Khatua and Patra 2008; Khatua et al. 2012). Distribution of boundary shear stress and depth average velocity mainly depends upon the shape of the cross-section and the structure of the secondary flow cells. However, for converging floodplain geometry, there is wide variation in the local shear stress distribution from point to point in the wetted perimeter. Also, the magnitude of boundary shear and depth average velocity of a converging channel is significantly different from that of straight channels having the same geometry, shape and cross-sectional area. Therefore, there is a need to evaluate the boundary shear stress and depth average velocity carried by the main channel and floodplain walls at various locations of contracted path. Conventional approaches lack in providing high accuracy for the prediction of the boundary shear in channels due to neglecting the factors causing non-uniformity of flow. This necessitates a new and accurate technique. The present research investigates some experimental findings of different converging compound channels of different geometry and converging angles. The effect of geometry and converging angle on flow prediction of such channels is studied and finally an efficient approach is proposed to estimate the boundary shear and depth average velocity with the help of artificial neural network (ANN) which is a promising computational tool. Some of the important past studies in this direction are neuro-fuzzy model to simulate Coolbrook White equation by Walid and Shyam (1998), prediction of friction factor in smooth open channel flow using ANN by Bigil and Altum (2008) and Yuhong and Wenxin (2009), prediction of discharge in straight compound open channel flow by Sahu et al. (2011), prediction of roughness coefficient of a meandering open channel flow using neuro-fuzzy inference system by Moharana and Khatua (2013), predicting apparent shear stress in prismatic compound open channels using artificial neural networks by Huai et al. (2013). Ebtehaj and Bonakdari (2013) utilized an MLP neural network to predict the minimum sediment transport velocity in sewers. The results indicated that the MLP neural network can quite accurately estimate the minimum velocity. Sun et al. (2014) investigated the capability of ANN to predict the velocity distribution in combined open channels using computational fluid dynamics data. Kızıloz et al. (2015) predicted scour around submarine pipelines using ANN and found that the ANN results are in good agreement with the measured data.

New experiments have been conducted at the Hydraulics and Fluid mechanics Laboratory of Civil Engineering

Department of NIT, Rourkela to analyse the behaviour of boundary shear and depth average velocity caused by floodplain contractions. An evaluation of the boundary shear and depth average velocity in different converging sections of a compound channel reach for different hydraulic and geometric conditions is done and the dependency of boundary shear and depth average velocity for such channels is analysed. An attempt is also made to develop a mathematical model based on ANN to predict the boundary shear and depth average velocity due to contraction effect and flow conditions for several converging compound channels. The results are compared with the experimental data of N.I.T Rourkela and Rezaei (2006).

2 Boundary Shear Stress Measurement

Shear studies in open channel flow have many implications such as bed load transport, channel migration, and momentum transfer. Bed shear forces are useful for the study of bed load transfer, whereas wall shear forces present a general view of the channel migration pattern. There are several methods used to evaluate bed and wall shear stress in an open channel. The Preston tube method is an indirect estimate for shear stress measurements and is widely used for the experimental channel which is described below.

Using Preston's technique together with calibration curves of Patels (1965), local boundary shear stress measurements were made around the wetted perimeter of the present converging channel. Preston developed a simple shear stress measurement technique for smooth boundaries in a fully developed turbulent flow using a Pitot tube. Preston presented a non-dimensional relationship between the differential pressures Δp and the boundary shear stress τ_w .

$$\frac{\Delta p}{\rho} \frac{d^2}{v^2} = F \left[\frac{d^2 \tau_w}{\rho v^2} \right] \quad (1)$$

where d is the outside diameter of the tube, ρ is the density of the flow, v is the kinematic viscosity of the fluid and F is an empirical function. Following this work, Patel (1965) presented definitive calibration curves for the Preston tube defined in terms of two non-dimensional parameters which are used to convert pressure readings to boundary shear stress.

$$x^* = \log_{10} \left(\frac{\Delta p d^2}{4 \rho v^2} \right) \quad (2)$$

$$y^* = \log_{10} \left(\frac{\tau_w d^2}{4 \rho v^2} \right) \quad (3)$$

The calibration of x^* and y^* for different regions of the velocity distribution (i.e., viscous sub layer, buffer layer and logarithmic layer) are expressed by three different formulae.

$$y^* = 0.5x^* + 0.037 \quad \text{for } 0 < y^* < 1.5 \quad (4)$$

$$y^* = 0.8287 - 0.1381x^* + 0.1437x^{*2} - 0.0060x^{*3} \quad \text{for } 1.5 < y^* < 3.5 \quad (5)$$

$$x^* = y^* + 2 \log_{10}(1.95y^* + 4.10) \quad \text{for } 3.5 < y^* < 5.3 \quad (6)$$

In the present case, all shear stress measurements are taken on all the five sections of the converging angles. The pressure readings were taken using Pitot tube. These are placed at the predefined points of the flow-grid in the channel, facing the flow which is demonstrated in Fig. 1c for in a bank and overbank flow conditions, respectively. The manometers attached to the respective Pitot tubes are used to measure the head difference. The differential pressure was then calculated from the readings on the vertical manometer.

$$\Delta P = \rho g \Delta h \quad (7)$$

where Δh is the difference between the two readings from the dynamic and static, g is the acceleration due to gravity and ρ is the density of water. Here the tube coefficient is taken as a unit and the error due to turbulence is considered negligible while measuring velocity. After that, the shear stress values were integrated over the entire perimeter to calculate the total shear force per unit length normal to flow cross-section carried by the compound section. The total shear thus computed was then compared with the resolved component of weight force of the liquid along the stream-wise direction to check the accuracy of the measurements. The error percentages are found out to be within $\pm 10\%$.

3 Tangential Velocity Measurement

In the present work velocity, readings are taken using Pitot tubes as well as 16-MHz Micro-ADV (Acoustic Doppler Velocity Meter) manufactured by M/s Son-Tek, San Diego, Canada. According to the laboratory data analysis, shear stress from a Pitot tube is the most appropriate shear stress calculation method as compared to ADV, as near the boundary, the velocity measurement ADV has never been accurate (Khatua 2008). Apart from this, ADV has some limitations of velocity measurements. It can measure 5 cm below its top edge. In down probe of micro-ADV, it could not measure 5 cm near the free surface. So, Pitot tube has been utilized to measure the short fall. The accuracy of this method has been verified from the energy gradient

approach, i.e., weight component of the flow. Pitot tubes are placed in the direction of flow and then allowed to rotate along a plane parallel to the bed and till a relatively maximum head difference appeared in manometers attached to the respective Pitot tubes. The deviation angle between the reference axis and the total velocity vector is assumed to be positive when the velocity vector is directed away from the outer bank. The total head h reading by the Pitot tube at the predefined points of the flow-grid in the channel is used to measure the magnitude of point velocity vector as $U = (2gh)^{1/2}$, where g is the acceleration due to gravity. Resolving U into the tangential and radial directions, the local velocity components are obtained. Here the tube coefficient is taken as a unit and the error due to turbulence is considered negligible while measuring the velocity. Here, head loss has been neglected. After finding the velocity from point to point, we have estimated the observed discharge by time rise method by volumetric tank. We have distributed the error uniformly to all the points. Point velocities were measured along verticals spread across the main channel and flood plain so as to cover the width of the entire cross-section. The depth-averaged velocity U_d is defined by the Eq. (8).

$$U_d = \frac{1}{H} \int_0^H U \, dy \quad (8)$$

U_d is a very important parameter along with the boundary shear stress in all compound channel flow studies and needs to be measured with sufficient accuracy to determine its distribution across the flow section with varying relative depth ($\beta = (H - h)/H$, where H = height of water at a particular section and, h = height of water in main channel) as well as for the estimation of unit discharge.

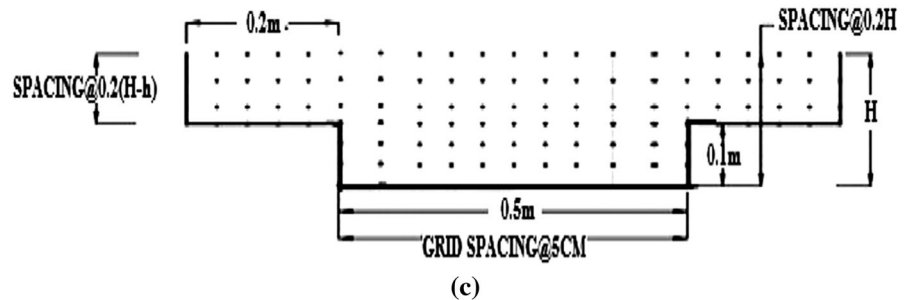
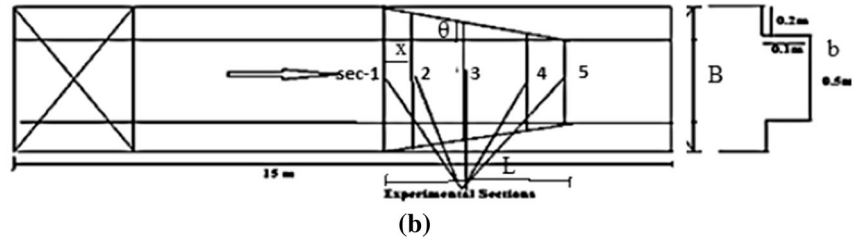
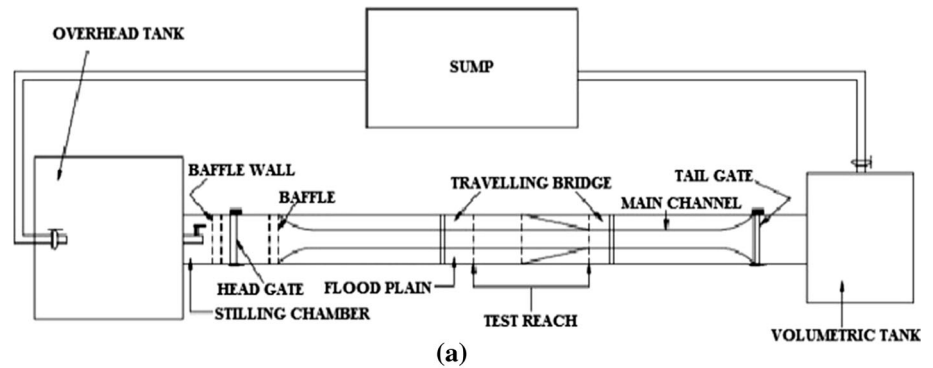
4 Sources of Data and Selection of Hydraulic Parameters

Along with the presently carried out experimental data set, an extensive literature related to the analysis of converging compound channels is also reviewed. The standard data set was collected from several is prepared in Table 1

4.1 Selection of Hydraulic, Geometric and Surface Parameters

Flow hydraulics and momentum exchange in converging compound channels are significantly influenced by both geometrical and hydraulic variables; the computation becomes more complex when the floodplain width contracts and become zero. The flow factors responsible for the

Fig. 1 **a** Plan view of experimental setup. **b** Longitudinal and cross-sectional dimension of the non-prismatic compound channels. **c** Typical grid showing the arrangement of velocity measurement points at the test section. **d** Photo of converging compound channel with movable bridge, pitot tube and pointer gauge



estimation of boundary shear stress and depth average velocity are

1. Converging angle denoted as θ .
2. Relative flow depth denoted as $\beta = (H - h)/H$. Where H = height of water at a particular section and, h = height of water in the main channel.
3. Width ratio (α), i.e., Ratio of width of floodplain to width of main channel.
4. Aspect ratio (σ), i.e., ratio of the width of the main channel to depth of main channel
5. Relative distance (Z_r), i.e., ratio of the distance between the two consecutive sections to the total contracted length of the non-prismatic channel.

Table 1 Hydraulic parameters for the experimental channel data set collected from literature and experiments

Verified test channel	Types of channel	Angle of convergent	Longitudinal slope (S)	Cross-sectional geometry	Total channel width (B) in m	Main channel width (b) in m	Main channel depth (h) in m	Main channel side slope (s)	Width ratio B/b (α)
1	2	3	4	5	7	8	9	10	11
Rezaei (2006)	Convergent (CV2)	$(\theta = 11.31^\circ, 2 \text{ m})$	0.002	Rectangular	1.2	0.398	0.05	0	3
Rezaei (2006)	Convergent (CV6)	$(\theta = 3.81^\circ, 6 \text{ m})$	0.002	Rectangular	1.2	0.398	0.05	0	3
Rezaei (2006)	Convergent (CV6)	$(\theta = 1.91^\circ, 6 \text{ m})$	0.002	Rectangular	1.2	0.398	0.05	0	3
N.I.T. Rkl data	Convergent	$(\theta = 5^\circ, 2.28 \text{ m})$	0.0011	Rectangular	0.9	0.5	0.1	0	1.8
N.I.T. Rkl data	Convergent	$(\theta = 9^\circ, 1.26 \text{ m})$	0.0011	Rectangular	0.9	0.5	0.1	0	1.8
N.I.T. Rkl data	Convergent	$(\theta = 12.38^\circ, 0.84 \text{ m})$	0.0011	Rectangular	0.9	0.5	0.1	0	1.8

5 Experimental Setup and Procedure

Experiments have been conducted in three sets of non-prismatic compound channels with varying cross-sections built inside a concrete flume measuring 15 m long \times 0.90 m width \times 0.5 m depth and flume with a Perspex sheet of the same dimensions. The width ratio of the channel is $\alpha = 1.8$ and the aspect ratio is $\sigma = 5$. The converging angles of the channels are taken as 12.38° , 9° and 5° , respectively. The converging length of the channels is found to be 0.84, 1.26, and 2.28 m, respectively. In a compound channel with converging floodplains, due to change in floodplain width, the flow condition is not uniform. Hence based on the downstream water depth imposed by tailgates, different water surface profiles in the upstream prismatic and the converging part of the flume can be observed. For each flume configuration of four different overbank flows (corresponding to the four relative flow depths $\beta = 0.15, 0.2, 0.25$ and 0.3 at the central reach) were tested. For each selected discharge, the downstream water level was adjusted, using the tailgate setting, in such a way that the backwater profile (M1 and M3 profile) was reached at a given depth at the central section of narrowing reach. To achieve this, for each non-prismatic compound channel configuration, a wide range of discharges was used. For each specific discharge, by changing the tailgate level various water surface profiles could be measured. When the channel bottom slope is less than the critical slope then it is called as mild slope, thus profiles that occur in mild slope are called M slopes. In mild slope condition

M1 and M3 profiles are backwater profiles which signify the slope of water as positive. Water was supplied through a series of centrifugal pumps (each 11,185.5-W capacity) discharging into a large RCC overhead tank. In the downstream end, there is a measuring tank followed by a sump which feeds the water to the overhead tank through pumping. This arrangement completes the recirculation system of water for the experimental channels. Figure 1a shows the plan view of experimental sections. Figure 1b shows the diagram of prismatic and non-prismatic test section. Consider a prismatic compound channel which has total width = B and main channel width of b . Let the floodplain be contracted from width B at section 1 to the width of b at section 5 as shown in Fig. 1b. It may be noted that total converging part of the channel has been divided into 5 arbitrary sections. Figure 1c shows the typical grid showing the arrangement of velocity measurement points along the horizontal and vertical direction of the test section. Figure 1d shows the photo of converging compound Channel with Movable Bridge, Pitot tube and Pointer gauge. At the downstream end, another adjustable tail gate was provided to control the flow depth and maintain a uniform flow in the channel. A movable bridge was provided across the flume for both span-wise and stream-wise movements over the channel area, so that each location on the plan of the compound converging channel could be accessed for taking measurements.

Point velocities were measured along verticals spread across the main channel and flood plain so as to cover the width of the entire cross-section. Measurements were thus

taken from the midpoint of the main channel to the left edge of the floodplain. The lateral spacing of grid points over which measurements were taken was kept 5 cm inside the main channel and the flood plain. Several runs were conducted for overbank flow with relative depth varying between 0.15 and 0.3. Table 1 shows the hydraulic parameters of different channels used in this paper. For the present analysis, we have also used the data of Rezaei (2006). Rezaei (2006) conducted experiments on different converging angles. Now we have evaluated the boundary shear stress and depth average velocity in the flow due to the convergence of floodplain at different sections of the converging lengths.

6 Experimental Results

The depth average velocity distribution of relative depth 0.3 for converging angle 12.38° and for relative depth 0.5 of the converging angle 11.31° (Rezaei 2006) are shown in Fig. 2a, b. From these figures, we can observe that the depth average velocity distributions are reasonably symmetric in all sections and gradually increase from Sec-1 to Sec-5. In all sections, the boundary shear value is found to be maximum in the middle of the main channel and gradually decreases towards the interface between the main channel and floodplain. The boundary shears distribution

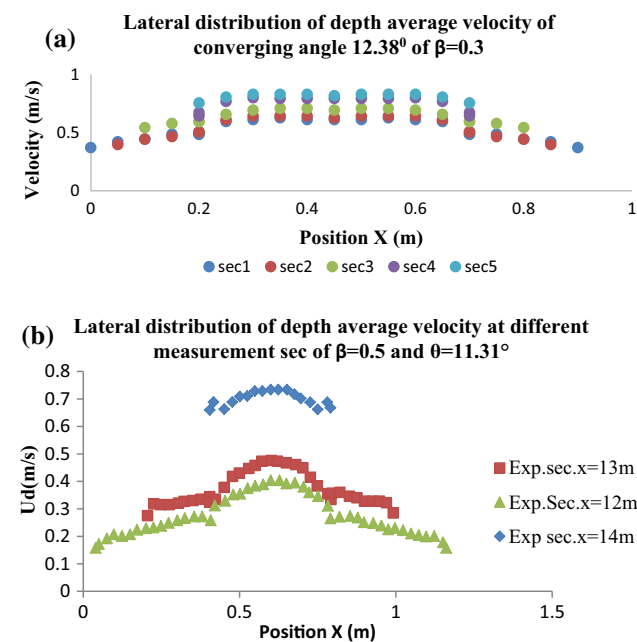


Fig. 2 a Depth average velocity distribution for present experimental channel of relative depth 0.3 (for converging angle 12.38°). b. Depth average velocity distribution for the Rezaei (Walid and Shyam 1998) experimental channel of relative depth 0.5 (for converging angle 11.31°)

for relative depth 0.15 for converging angle 12.38° and for relative depth 0.5 of the converging angle 11.31° (Rezaei 2006) is shown in Fig. 3a, b. These figures indicate that the boundary shear stress distributions are reasonably symmetric in all sections and gradually increase from Sec-1 to Sec-5. In all sections, the boundary shear value is found to be maximum in the middle of the main channel and gradually decreases towards the interface between the main channel and floodplain. At the interface the boundary shear suddenly falls, then it decreases and reaches the minimum at both ends of floodplains. This may be due to momentum transfer phenomena between the main channel and floodplains. Similarly, this happens to the converging channel of Rezaei (2006) with angle 11.31° . However, at the last section of Rezaei (2006), maximum boundary shear are found to occur at the two ends of the main channel instead of the middle of the main channel. Because the last section is the single channel with higher aspect ratio, as compared to the present experimental channel.

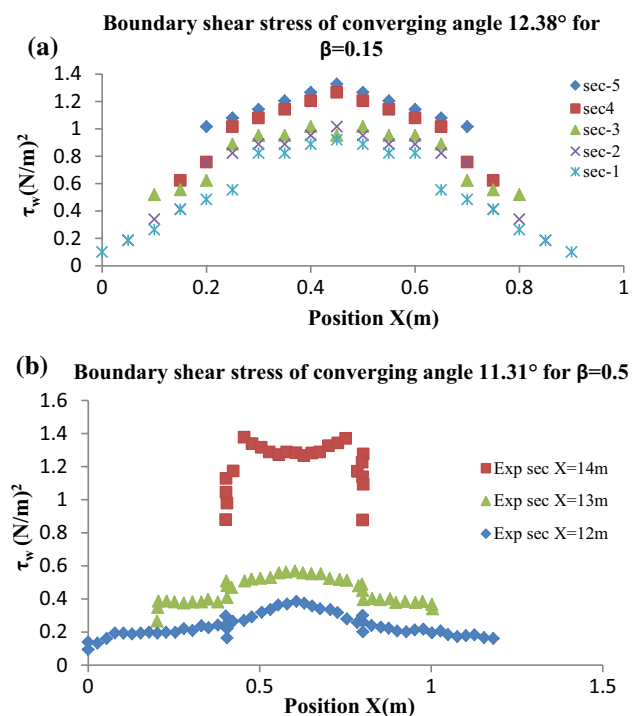


Fig. 3 a Boundary shear distribution for the present experimental channel of relative depth 0.15 (for converging angle 12.38°). b Boundary shear distribution for the Rezaei (Walid and Shyam 1998) experimental channel of relative depth 0.5 (for converging angle 11.31°)

7 Artificial Neural Network

ANN is a new and rapidly growing computational technique. In recent years, it has been broadly used in hydraulic engineering and water resources. It is a highly self-organised, self-adapted and self-trainable approximator with high associative memory and nonlinear mapping. ANNs may consist of multiple layers of nodes interconnected with other nodes in the same or different layers. The various layers are referred to as the input layer, the hidden layer, and the output layer. The inputs and the interconnected weights are processed by a weight summation function to produce a sum that is passed to a transfer function. The output of the transfer function is the output of the node. In this paper multi-layer perception network is used. Input layer receives information from the external source and passes this information to the network for processing. Hidden layer receives information from the input layer and does all the information processing, and output layer receives processed information from the network and sends the results out to an external receptor. The input signals are modified by interconnection weight, known as weight factor W_{ij} which represents the interconnection of i th node of the first layer to the j th node of the second layer. The sum of modified signals (total activation) is then modified by a sigmoidal transfer function (f). Similarly, output signals of hidden layer are modified by interconnection weight (W_{ij}) of the k th node of the output layer to the j th node of the hidden layer. The sum of the modified signal is then modified by a pure linear transfer function (f) and output is collected at the output layer.

7.1 Sigmoidal Function

A bounded, monotonic, non-decreasing, S shaped function provides a graded nonlinear response. It includes the logistic sigmoid function

$$F(x) = \frac{1}{1 + e^{-x}} \quad (9)$$

where x = input parameters taken

The architecture of back propagation neural network model, that is the 1- m - n (l input neurons, m hidden neurons, and n output neurons) is shown in Fig. 4.

7.2 Learning or Training in Back Propagation Neural Network

Batch mode type of supervised learning has been used in the present case in which interconnection weights are adjusted using delta rule algorithm after sending the entire training sample to the network. During training, the predicted output is compared with the desired output and the

mean square error is calculated. If the mean square error is more, then a prescribed limiting value is back propagated from output to input and weights are further modified till the error or number of iteration is within a prescribed limit.

Mean squared error, E_p for pattern p is defined as

$$E_p = \sum_{i=1}^n \frac{1}{2} (D_{pi} - O_{pi})^2 \quad (10)$$

where D_{pi} is the target output, O_{pi} is the computed output for the i th pattern.

Weight changes at any time t is given by

$$\Delta W(t) = -nEp(t) + \alpha \times \Delta W(t-1) \quad (11)$$

n = learning rate, i.e., $0 < n < 1$; α = momentum coefficient, i.e., $0 < \alpha < 1$.

8 Results and Discussions

8.1 Testing of Back Propagation Neural Network

The total experimental data sets of both boundary shear stress and depth average velocity are divided into training set and testing set. The experimental data sets contain three converging angles, five different sections of each converging angle and four relative depths each converging angle and different section of Rezaei (2006) along with three converging angles of NIT Rourkela channels. Details of all the experimental data are given in Table 1. For boundary shear stress calculations, 12,298 data are used, among which 70% are training data and 30% are taken as testing data. For depth average velocity calculations, 24,196 data are used, among which 70% data are used training and 30% are taken as testing data. The number of layers and neurons in the hidden layer are fixed through exhaustive experimentation when mean square error is minimized for training data set. It is observed that minimum error is obtained for 5-7-1 architecture. So, the back propagation neural network (BPNN) used in this work has three layered feed forward architecture. The model was run on MATLAB commercial software dealing with trial and error procedure.

A regression curve is plotted between actual and predicted boundary shear stress, which is shown in Figs. 5 and 6. It can be observed that data for both cases are well-fitted because a high degree of the coefficient of determination, R^2 of 0.964 is obtained for the boundary shear stress calculations and R^2 of 0.977 is obtained for the depth average velocity between the sections. The residual analysis is carried out by calculating the residuals from the actual boundary shear stress and predicted boundary shear stress data. The residual testing and training data are plotted

Fig. 4 The architecture of back propagation neural network model

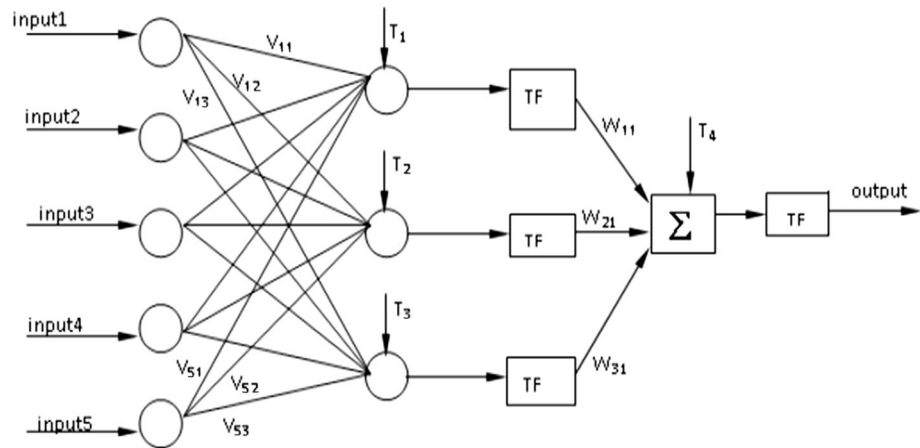
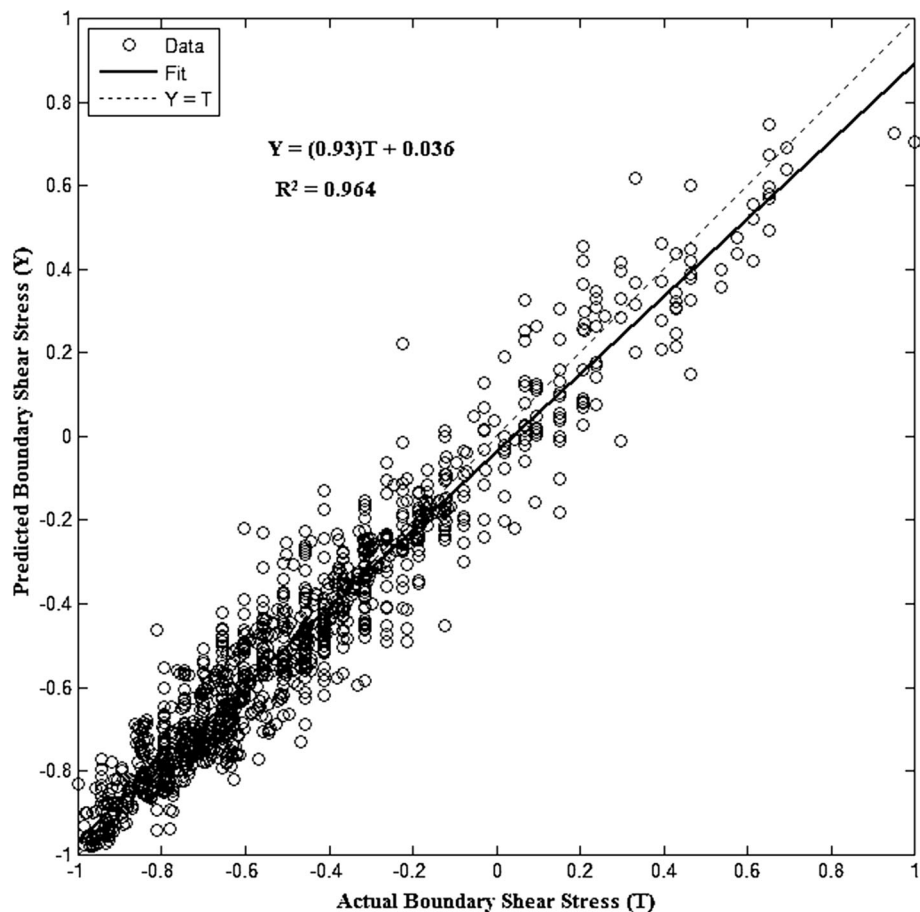


Fig. 5 Correlation plot of the actual boundary shear stress and predicted boundary shear stress



against the sample number as shown in Figs. 7 and 8, which shows that the actual data and predicted boundary shear stress against the sample number follows the same pattern with little or no exception; this demonstrates that the model predicts the pattern of the data distribution with adequate accuracy.

The actual depth average velocity and predicted depth average velocity training data against the sample number is shown in Fig. 9. Similarly, the actual depth average

velocity and predicted actual depth average velocity testing data against the sample number is shown in Fig. 10. Figures 9 and 10 follow the same pattern with little or no exceptions; it demonstrates that the model predicts the pattern of the data distribution with adequate accuracy. To check the strength of the model, error analyses have been done. Mean absolute error (MAE), the mean absolute percentage error (MAPE), mean squared error (MSE), the root mean squared error (RMSE) for all the converging

Fig. 6 Correlation plot of actual depth average velocity and predicted depth average velocity

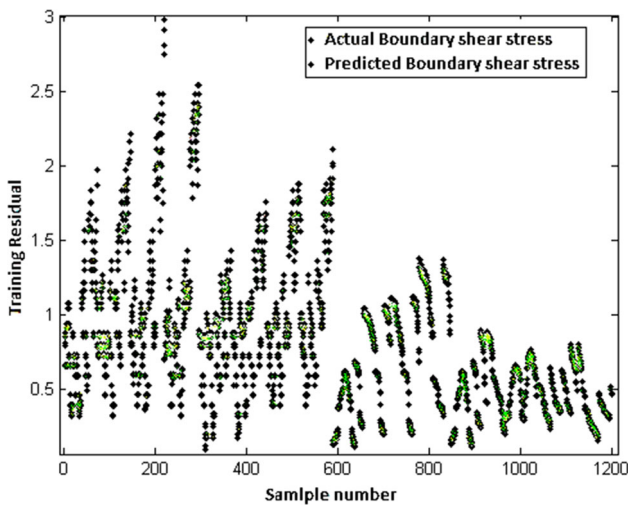
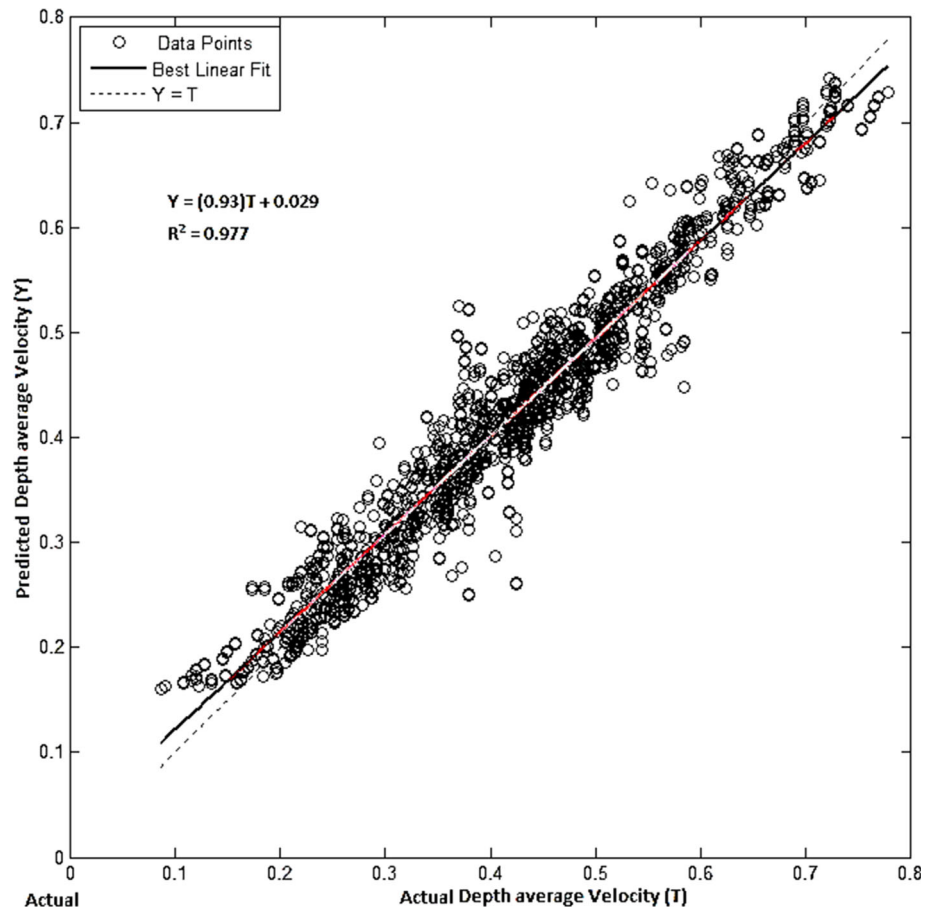


Fig. 7 Comparison of actual and predicted boundary shear stress (training data)

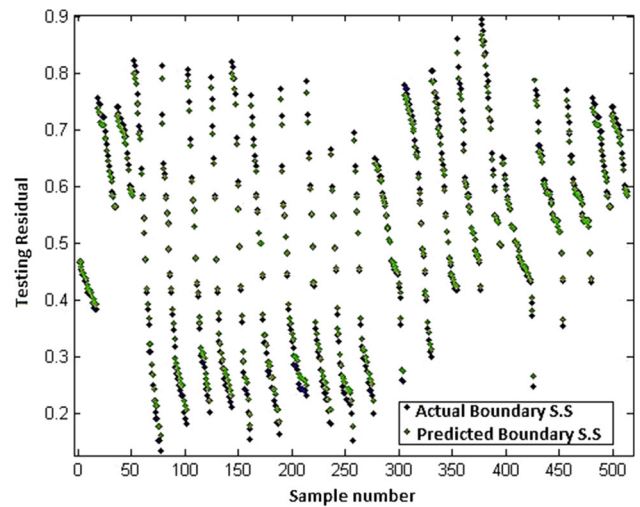


Fig. 8 Comparison of actual and predicted boundary shear stress (testing data)

compound channels for different flow conditions have been estimated. The statistical results of empirical equations in predicting boundary shear stress and depth average velocity are shown in Table 2.

The definitions of error terms are described below.

8.1.1 Mean Absolute Error (MAE)

The mean absolute error has been evaluated as,

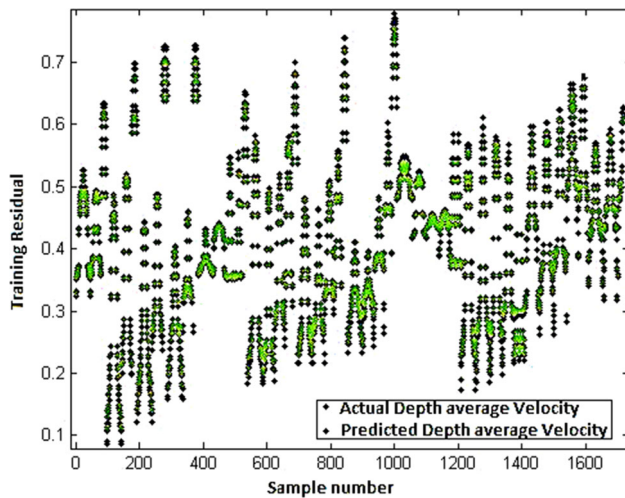


Fig. 9 Comparison of actual and predicted depth average velocity (training data)

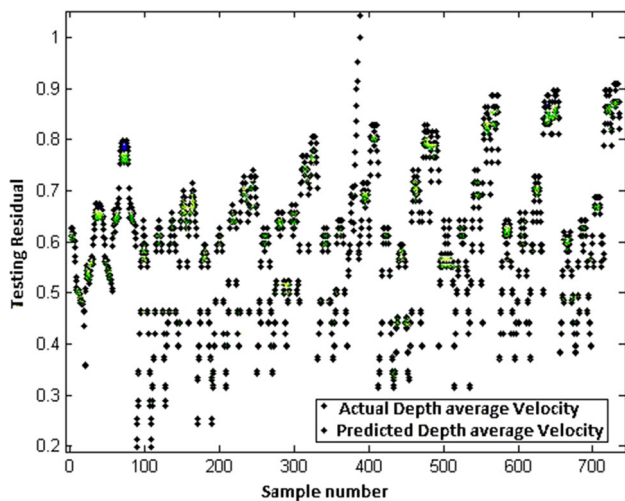


Fig. 10 Comparison of actual and predicted depth average (testing data)

Table 2 Statistical results of empirical equation in predicting boundary shear stress and depth average velocity

Error calculations	Boundary shear stress	Depth average velocity
MSE	0.001196	0.000255
RMSE	0.034577	0.015958
MAE	0.023199	0.012193
MAPE	3.33	2.40

$$\text{MAE} = \frac{1}{n} \sum_i^n \left| \frac{P_i - O_i}{O_i} \right| \quad (12)$$

where P_i = predicted values, O_i = observed values

Mean absolute error (MAE) measures how far predicted values are away from observed values. Thus, the minimum deviation of the predicted value from the observed value will obtain a better the result.

8.1.2 Mean Absolute Percentage Error (MAPE)

Mean absolute percentage error also is known as mean absolute percentage deviation is usually expressed as a percentage and is defined by the formula

$$\text{MAPE} = \frac{1}{n} \sum_i^n \left| \frac{O_i - P_i}{O_i} \right| \quad (13)$$

If mean percentage deviation of the predicted value from the observed value is within 10% then the model can be regulated as a good prediction model.

8.1.3 Mean Squared Error (MSE)

Mean squared error measures the average of the squares of the errors. It is computed as

$$\text{MSE} = \frac{1}{n} \sum_i^n (P_i - O_i)^2 \quad (14)$$

The MSE value zero signifies that the estimated data of the observed parameter is likely to be most accurate or ideally best. Since it is difficult to achieve zero value, it is seen that the closest value to zero is reasonably acceptable.

8.1.4 Root Mean Squared Error (RMSE)

Root mean squared error or root mean squared deviation is also a measure of the differences between values predicted by a model or an estimator and the actually observed values. These individual differences are called as residuals when the calculations are performed over the data sample that is used for estimation and are known as estimation errors when computed out of the sample. The RMSE is defined as,

$$\text{RMSE} = \sqrt{\text{MSE}} \quad (15)$$

When two data sets, i.e., one set from theoretical prediction and the other from actual measurement of some physical variable (which in our case is observed versus predicted) are compared, the RMSE of the pairwise deviation among the two data sets can function as a measure of how far on average the error is from 0.

9 Conclusions

Prediction of boundary shear stress and depth average velocity of converging compound channels are found to depend on upon a number of hydraulic and geometrics out of which aspect ratio, depth ratio, width ratio, relative distance, converging angle and relative depth are the most influencing non-dimensional parameters.

An ANN model is proposed for accurate estimation of boundary shear stress and depth average velocity of converging compound channels. The trend and pattern of experimental data match with boundary shear stress and depth average velocity. The basic reason of high degree of prediction accuracy lies in the fact of the capability of nonlinear mapping of inputs and outputs in a neural network system. The nonlinear relation of geometrical and hydraulic input parameters with boundary shear stress and depth average velocity data are difficult to establish with any traditional boundary shear stress and depth average velocity data prediction methodology. It can be inferred that this model is more adaptive to the prediction of boundary shear stress and depth average velocity under different conditions.

ANN model holds the boundary shear stress prediction with minimal error, i.e., MSE as 0.001196 RMSE as 0.034577, MAE as 0.023199 and MAPE 3.33 which is less than 10%. Similarly for depth average velocity MSE as 0.00025, RMSE as 0.015958, MAE as 0.012193 and MAPE 2.40 which is also less than 10%. So, the present ANN model is a more convincing model.

Acknowledgements The author wishes to thankfully acknowledge the support from the Institute and the UGC UKIERI Research project (Ref No. UGC-2013 14/017) and for carrying out the research work in the Hydraulics Laboratory at National Institute of Technology, Rourkela is thankfully acknowledged by the second author.

References

- Bigil A, Altun H (2008) Investigation of flow resistance in smooth open channels using artificial neural network. *Flow Meas Instrum* 19:404–408
- Bousmar D, Wilkin N, Jacquemart JH, Zech Y (2004) Overbank flow in symmetrically narrowing floodplains. *J Hydraul Eng ASCE* 130(4):305–312
- Ebtehaj I, Bonakdari H (2013) Evaluation of sediment transport in sewer using artificial neural network. *Eng Appl Comput Fluid Mech* 7:382–392
- Ghosh SN, Jena SB (1971) Boundary shear distribution in open channel compound. *Proc Inst Civ Eng Lond* 49:417–430
- Huai W, Chen G, Zeng Y (2013) Predicting apparent shear stress in prismatic compound open channels using artificial neural networks. *J Hydraul Eng* 15(1):138–146
- Khatua KK (2008) Interaction of flow and estimation of discharge in two stage meandering compound channels. Thesis Presented to the National Institute of Technology, Rourkela, in partial fulfillments of the requirements for the Degree of Doctor of Philosophy
- Khatua KK, Patra KC (2008) Boundary shear stress distribution in compound open channel flow. *J Hydraul Eng* 12(3):39–55
- Khatua KK, Patra KC, Mohanty PK (2012) Stage-discharge prediction for straight and smooth compound channels with wide floodplains. *J Hydraul Eng* 138(1):93–99
- Kızıllöz B, Çevik E, Aydoğan B (2015) Estimation of scour around submarine pipelines with artificial neural network. *Appl Ocean Res* 51:241–251
- Moharana S, Khatua KK (2013) Prediction of roughness coefficient of a meandering open channel flow using neuro-fuzzy inference. *Flow Meas Instrum* 51:112–123
- Myers WRC (1987) Velocity and Discharge in Compound Channels. *J. Hydraul. Eng. ASCE* 113(6):753–766
- Patel VC (1965) Calibration of the Preston tube and limitations on its use in pressure gradients. *J Fluid Mech* 23:185–208
- Patra KC (2004) Flow and velocity distribution in meandering compound channels. *J Hydraul Eng* 130(5):398–411
- Patra K, Kar SK (2000) Flow interaction of meandering river with flood plains. *J Hydraul Eng* 126(8):593–603
- Proust S, Rivière N, Bousmar D, Paquier A, Zech Y (2006) Flow in the compound channel with abrupt floodplain contraction. *J Hydraul Eng* 132(9):958–970
- Rezaei B (2006) Overbank flow in compound channels with prismatic and non-prismatic floodplains. PhD Thesis University of Birmingham, UK
- Rezaei B, Knight DW (2011) Overbank flow in compound channels with non-prismatic floodplains. *J Hydraul Res* 137:815–824
- Rhodes DG, Knight DW (1994) Distribution of shear force on boundary of smooth rectangular duct. *J Hydraul Eng* 120–7:787–807
- Sahu M, Khatua KK, Mahapatra SS (2011) A neural network approach for prediction of discharge in straight compound open channel flow. *Flow Meas Instrum* 22:438–446
- Sun S, Yan H, Kouyi GL (2014) Artificial neural network modelling in simulation of complex flow at open channel junctions based on large data sets. *Environ Model Softw* 62:178–187
- Walid HS, Shyam SS (1998) An artificial neural network for non-iterative calculation of the friction factor in pipeline flow. *Comput Electron Agric* 21:219–228
- Yuhong Z, Wenxin H (2009) Application of artificial neural network to predict the friction factor of the open channel. *Commun Nonlinear Sci Numer Simul* 14:2373–2378